REPORT DOCUMENTATION PAGE

Form Approved
OMB No. 0704-0188

1. REPORT DATE *(DD-MM-YYYY)*	2. REPORT TYPE	3. DATES COVERED *(From - To)*
20-01-2010	Final Technical Report	June 2009 - January 2010

4. TITLE AND SUBTITLE

Hazardous Particle Detection via Unmanned Air Vehicles: Optimal Placement of Sensors in Forward Flight

5a. CONTRACT NUMBER
W31P4Q-09-C-0548

5b. GRANT NUMBER

5c. PROGRAM ELEMENT NUMBER

6. AUTHOR(S)
Drs. Peter S. Bernard and Jacob Krispin

5d. PROJECT NUMBER

5e. TASK NUMBER

5f. WORK UNIT NUMBER

7. PERFORMING ORGANIZATION NAME(S) AND ADDRESS(ES)
Vorcat, Inc
14 Freas Court
North Potomac, Maryland 20878

8. PERFORMING ORGANIZATION REPORT NUMBER
TR-10-0001

9. SPONSORING/MONITORING AGENCY NAME(S) AND ADDRESS(ES)
Defense Advanced Research Projects Agency
Suite 120
3701 Fairfax Drive, Arlington, VA 22203-1700

10. SPONSOR/MONITOR'S ACRONYM(S)
DARPA

11. SPONSOR/MONITOR'S REPORT NUMBER(S)

12. DISTRIBUTION/AVAILABILITY STATEMENT
Approved for public release, distribution unlimited

13. SUPPLEMENTARY NOTES

14. ABSTRACT

This project explores means of enhancing the efficiency of bio/chem/nuclear hazard detection in the atmosphere by unmanned air vehicles (UAV). Specifically, the study seeks to discover if and where the placement of sensors on UAV's can maximize the volume of space that is brought into contact with the sensor. A hybrid gridfree/finite volume numerical flow simulation methodology that is adept at modeling complex flow scenarios provides the basis for the analysis. This study focuses on the use of an unmanned helicopter in collecting particle data. Clear evidence is found that the judicious placement of sensors on the UAV can profoundly affect the efficiency with which the atmosphere can be surveyed for hazards. In particular, for the geometry considered here, sensor placement in the tail section of a helicopter in forward flight is found to enable sampling particles that originate from relatively widely separated forward positions. Future work should be devoted to optimizing sensor placement for particular geometries under a range of flight conditions.

15. SUBJECT TERMS

16. SECURITY CLASSIFICATION OF:			17. LIMITATION OF ABSTRACT	18. NUMBER OF PAGES	19a. NAME OF RESPONSIBLE PERSON
a. REPORT	b. ABSTRACT	c. THIS PAGE			Jacob Krispin
U	U	U	UU		19b. TELEPHONE NUMBER *(Include area code)* 301-762-5553

445

Advanced Development for Defense Science and Technology

January 20, 2010

Sponsored by

Defense Advanced Research Projects Agency (DOD)
(Controlling DARPA Office)

Under ARPA Order AX11-00

Issued by U.S. Army Aviation and Missile Command

Contract No. W31P4Q-09-C-0548

Prepared By:
Dr. Jacob Krispin, PI

Vorcat, Inc.
14 Freas Court
North Potomac, MD 20878
Tel. (301) 762-5553
email: jacob@vorcat.com
Home Page: www.vorcat.com

SBIR Phase I Final Report

Title: Hazardous Particle Detection via Unmanned Air Vehicles: Optimal Placement of Sensors in Forward Flight

Period Covered: June 26, 2009 - January 20, 2010

Abstract

This project explores means of enhancing the efficiency of bio/chem/nuclear hazard detection in the atmosphere by unmanned air vehicles (UAV's). Specifically, the study seeks to discover if and where the placement of sensors on UAV's can maximize the volume of space that is brought into contact with the sensor. A hybrid gridfree/finite volume numerical flow simulation methodology that is adept at modeling complex flow scenarios provides the basis for the analysis. This study focuses on the use of an unmanned helicopter in collecting particle data. Clear evidence is found that the judicious placement of sensors on the UAV can profoundly affect the efficiency with which the atmosphere can be surveyed for hazards. In particular, for the cases considered thus far, sensor placement in the tail section of the helicopter in forward flight is found to enable sampling particles that originate from relatively widely separated forward positions. Future work should be devoted to optimizing sensor placement for particular geometries under a range of flight conditions.

Summary

Practical scenarios were explored for maximizing the efficiency with which unmanned air vehicles, specifically helicopters, can be used to sample the atmosphere for chem/bio/nuclear hazards. Simulation of particle flows encountered by a helicopter in forward flight were carried out using the VorCat code. A singularly effective means of accomplishing the project goals was identified: particles arriving at the rear tail section of the helicopter air frame are found to have a tendency to originate in widely separated forward positions. Placement of particle sensors in this location will be most efficient in sampling the atmosphere. The methodology developed here can be extended to provide detailed recommendations for sensor placement in specific helicopter geometries and flow conditions.

1 Introduction.

The detection of hazardous airborne chem/bio/nuclear particulates via sensors carried by unmanned air vehicles (UAV's) provides a potentially safe and effective means of gaining valuable time for mitigating or minimizing the consequences of such hazards to civilian and military populations. An important part of this technology is optimizing the efficiency with which the atmosphere can be scanned, a goal that is synonymous with maximizing the region of the atmosphere from which particles might arrive at the on board sensors. This project considers how the complex, turbulent vortical flows produced by UAV's can be harnessed for this purpose.

The effectiveness of current point source airborne testing for hazardous particles using UAV's is limited by the need to directly intersect the particles along the flight path

[1, 12, 19]. This lack of efficiency translates into extended flight times and the potentiality for mission failure in which dangerous particles are overlooked [15]. While it is possible to force increased airflow through sensors, (e.g. by the use of fans [20]) it is not evident that this necessarily increases the search volume in the surrounding air space. The focus of this project is in finding strategies for creating the largest possible sampling footprint of the UAV as it flies thus enhancing efficiency and accuracy in the search for dangerous particles.

The feasibility of this study is suggested by the tendency of UAV flow fields [14, 18] to include a range of complex flow phenomena that may include vortices associated with separated flow and vehicle maneuvering, vortex breakdown, shear layer instabilities and other effects. Vortex motions are also intrinsic to flow control efforts including micro-electro mechanical (MEMS) devices. Flow fields containing vortices and turbulence are noteworthy for their ability to promote dispersion and by so doing may bring particles within range of the intake of the airborne sensor that would otherwise be overlooked. While turbulence may strongly promote particle dispersion, the extent and nature of the effect varies depending on the volume and weight of the particles. In some cases, the effect of turbulence can be quite specific [22, 16, 11] and potentially useful in data collection. Thus, an important additional consideration in the project is to discern what kinds of particles are likely to be most advantageously brought to the sensor by specific strategies for air collection.

For the goals of the project to be attainable, a numerical scheme is required that can on the one hand accurately represent the complex, non-steady eddying motion associated with UAV's and on the other capture the essential dynamics of how airborne particles of different sizes and weights disperse within the turbulent flow environment. Since unsteadiness is an essential aspect of the physics, it is natural to use a Large Eddy Simulation (LES) method to represent the flow [2] since this offers the best prospect for reduced modeling at an affordable cost. Among LES alternatives, the gridfree vortex filament scheme devised by VorCat, Inc. is unique in its ability to capture the physical dispersion of particulates without the unphysical effects of imposed or unwanted small scale diffusion that is the hallmark of traditional grid-based LES schemes. The availability of this new methodology is an important factor in believing that the goals of the project are feasible.

The use of gridfree vortical elements provides VorCat with a direct representation of the essential physical properties of turbulent flow. This promotes a significant gain in numerical efficiency since the vortices that form the primary structure of turbulence are modeled directly without the intervention of a numerical mesh. Moreover, it is the absence of a mesh that removes the primary source of numerical diffusion in computational fluid dynamics (CFD) schemes. A number of validation studies [3, 4, 5, 6, 8] have demonstrated the capabilities of the VorCat approach and suggest that it is well suited for the proposed work. For example, the VorCat scheme has the property that it is applied the same to all flow situations: it does not require the selection of modeling parameters

whose precise values determine whether or not important physical trends are captured.

2 Methods, Assumptions, and Procedures

This study is based on the opportunities for analysis and simulation of complex flows provided by the VorCat, Inc. hybrid gridfree/finite volume flow solver. An overview of the technology is provided here including a discussion of how it is applied to the particular flow of interest in the present project.

2.1 Overview of the VorCat Methodology.

Vortex Tubes. Straight vortex tubes forming filaments are the gridfree elements used in VorCat. The ith tube is identified via its end points $\mathbf{x}_i^1, \mathbf{x}_i^2$ and circulation Γ_i. Vortex stretching and reorientation as contained in the governing vorticity transport equation are accommodated by convecting the tube end points according to the local velocity field. Tubes that stretch beyond a maximum length h are subdivided. The circulation of the tubes is assumed to remain constant in time owing to Kelvin's theorem: a reasonable approximation for high Reynolds number flow away from boundaries. Stretching and folding of the vortex tubes carries energy to small dissipative scales. Small vortex loops that naturally form are removed [4, 9, 10], thus providing a model of small scale local energy dissipation that is non-diffusive and essential for numerical efficiency.

Finite Volume Scheme. Since solid boundaries are where new vorticity is commonly produced in turbulent flow fields, it is vitally important to accurately simulate this process as part of the VorCat algorithm. Consequently, VorCat employs a high resolution finite volume scheme applied to the complete 3D viscous vorticity equation to compute the flow adjacent to walls. Solid surfaces are represented through triangularizations, out of which a thin mesh of triangular prisms is grown by erecting perpendiculars at the nodal points. The number of layers is usually taken to be 11 with the first layer of half-thickness. The prisms ideally have aspect ratio of 10. The thickness of the mesh region is designed to encompass the high vorticity and its gradients that are produced next to solid walls via viscosity. This region generally constitutes the viscous sublayer and an immediately adjacent part of the turbulent boundary layer. The no-slip condition is used to evaluate vorticity at the surface. Vorticity that convects and diffuses to the top sheet layer is turned into new vortex tubes. Details of the finite volume scheme may be found in recent articles [7, 8].

Velocity Field The vorticity residing in the tubes and in triangular prisms contributes to the velocity field as a sum of the contributions from individual elements according to the Biot-Savart law [21]. For the ith tube segment, the smoothed velocity field induced

at a point $\mathbf{x}$ may be computed from

$$-\frac{\Gamma_i}{4\pi}\frac{\mathbf{r}_i \times \mathbf{s}_i}{|\,\mathbf{r}_i\,|^3}\,\phi(r/\sigma) \tag{1}$$

where Γ_i is the circulation, $\mathbf{r}_i = \mathbf{x}_i - \mathbf{x}$, $r = |\,\mathbf{r}\,|$, $\phi(r) = 1 - \left(1 - \frac{3}{2}r^3\right)e^{-r^3}$ is a high order smoothing function, $\mathbf{s}_i$ is the axial vector along the segment and σ is a scaling parameter. In the case of sheets, the velocity field due to the ith sheet is determined by integrating the Biot-Savart kernel over the prism volume. These exact formulas are used in local calculations, and the prisms are regarded as additional tubes for more distant contributions. To enforce inflow and outflow boundary conditions or the non-penetration boundary condition at solid walls, a grid-free potential flow solution belonging to a surface source distribution is added to the velocity due to tubes and prisms. An advanced, parallel implementation of the Fast Multipole Method (FMM) [13] is used to compute the velocity produced by the N vortices and prisms in $O(N)$ operations.

Validation Studies. A variety of basic flow have been studied using VorCat in the interest of validating the technology. Computation of an isotropic turbulent field [4] established the capabilities of the method in capturing a range of fundamental flow statistics including spectra, correlation and structure functions. A subsequent computation of the spatially developing mixing layer [5] has provided the most comprehensive simulation of this important flow to date. A significant accomplishment of this work is providing an accurate portrayal of the flow from laminar inlet, through the development of vortical structures in transition to a fully turbulent self-similar region. Computed statistics and structural aspects of the mixing layer match previous physical experiments.

Similar accuracy has been achieved in the simulation of a co-flowing jet [6] and most recently in an investigation of the turbulent boundary layer [7, 8]. The latter is notable for capturing the complete transition including Blasius and turbulent log law velocity profiles. Moreover, the unique view of the boundary layer structure offered by vortex filaments, that give information about the orientation and organization of the vorticity field, has provided significant new insights into how the boundary layer is organized and evolves.

2.2 Helicopter Flow Including Particulates.

After discussions with Boeing, Inc. the decision was made to limit the type of unmanned air vehicles considered in the Phase I study to unmanned helicopters since these offer the greatest opportunity for harnessing the properties of the local flow field to accomplish the goals of the study. In this proof-of-concept study a generic helicopter shape is used to represent the air frame in the calculations and the rotor is modeled by introducing new vorticity from the blade tips as they rotate. An arbitrary number of blades can be specified as well as a continuous ring of vorticity in the limit of an infinite number

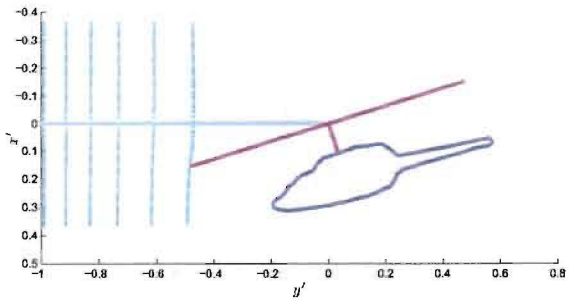

Figure 1: Side view of the problem setup. Outline of generic helicopter shape is blue, rotor plane and axis is red, flight direction is green and planes of particles released every 40 time steps (approximately 0.2 time units) upstream of the helicopter are cyan.

of blades as in the actuator disk model. Figure 1 shows the general setup as viewed from the side. The green horizontal line indicates the direction of flight, the rotor disk is red and circular planes of particles upstream of the helicopter are cyan. Calculations are performed in a reference frame fixed to the helicopter with the planes of particles released periodically every 40 time steps of the computation. The passage of the particles through the flow field produced by the rotor and helicopter body shape is computed and analyzed to determine an optimal placement of the particle sensor.

The velocity field is scaled by the nominal velocity just downstream of the rotor so this is unity in the computational problem. For the results discussed here the helicopter is tilted at an angle of 17.7^o from the horizontal with the consequence that the helicopter experiences a flow of 0.2 normal to the rotor disk outside its circumference and a flow 0.625 tangent to the rotor disk plane. In the case of an actuator disk, vorticity is shed into the flow at the circumference of the rotor in the form of vortex rings. For this case as well as computations with a finite number of blades, the vorticity shed from the rotor tips is decomposed into 5 separate vortex tubes of approximately equal circulation. For the actuator disk, the vortex rings entering the flow at each time step are composed of 40 straight segments. For the discrete rotor blades, vortex filaments with one end attached to the blade tips are introduced at each time step. Their length is proportional to the time step itself. The circulation strength of the vortices is determined by consideration of the total shearing between the velocity at the inside and outside of the rotor disk at its circumference.

The helicopter air frame used in the study is represented by 7450 triangles and the Reynolds number is 50,000. The finite volume mesh is 0.005 thick and covered by 11 layers of prisms. The use of a relatively coarse mesh is justified by the goals of this preliminary calculation. In future engineering work it can be anticipated that considerably finer surface meshes that contain more detail and allow for treatment of higher Reynolds numbers will be utilized.

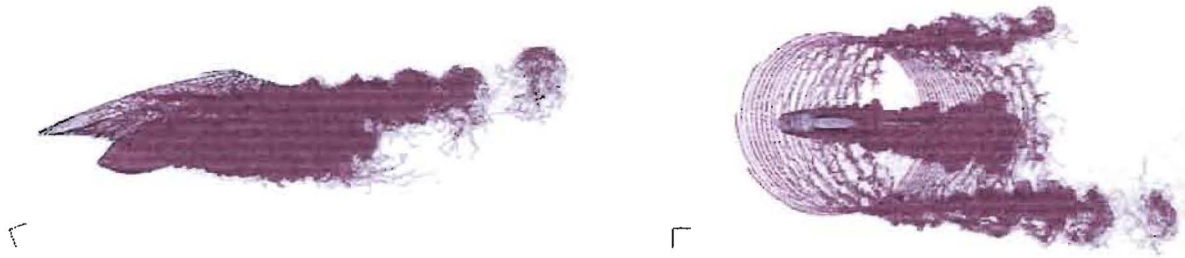

(a) Side view.

(b) Top view.

Figure 2: Vortex filaments produced in equilibrium by rotor (10 blades) and helicopter body in forward flight.

Vortex tubes enter the calculation both from the actuator disk and from vorticity produced in satisfaction of the non-slip condition on the surface of the helicopter. The latter tubes enter the flow at the top of the finite volume mesh covering the helicopter. To aid in numerical efficiency, vortex filaments that travel past a plane sufficiently far from the helicopter are removed from the computation.

Particle densities in the calculations are assumed to be sufficiently sparse that the carrier flow is unaffected by their presence. In this one-way coupling scenario the particle motion is determined using an empirical drag law appropriate to turbulent flow. The only necessary input is a Stokes number, S_t. Simulations for $S_t = 0$ (tracers) to heavy particles with $S_t = 100$ have been computed.

3 Results and Discussion.

Calculations of the helicopter flow are initiated from rest by impulsively adding the constant velocities in the directions parallel and normal to the rotor plane that are associated with forward flight. For a typical computation that had 10 rotor blades, equilibrium conditions in the number of vortex tubes is reached in approximately 400 time steps covering an elapsed time of 1.5. For the particular conditions in this case there are approximately 1.5M vortices at equilibrium. A calculation with the actuator disk reached equilibrium in a similar time scale and contained 2.4M vortices. Figure 2 gives two views of the vortex tubes at equilibrium for the 10 blade rotor calculation. The side view Fig. 2(a) shows the tilted rotor plane from which vortices trail out helically from the moving rotor with five vortices appearing at the tip of each blade. Contraction of the vortex wake is evident as well as the eventual degeneration into turbulence. At the same time vorticity formed over the air frame sheds forming a vortical wake, as well. A view from above in Fig. 2(b) shows more clearly the arrangement of vortices leaving the rotor blades and the breakup of the rotor field structure below the helicopter body.

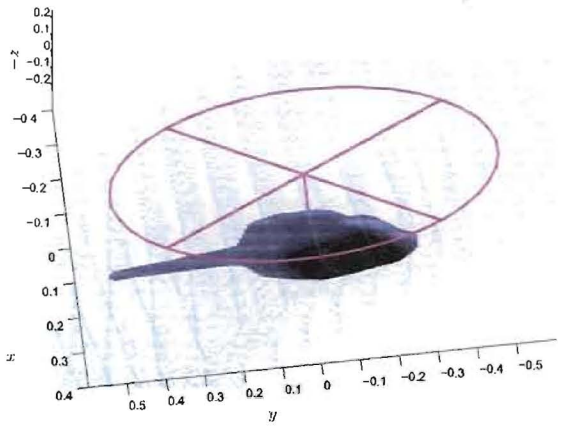

Figure 3: Circular planes of tracer particles impacting helicopter/rotor flow field. Particles are uniformly distributed on incoming planes.

Some idea of the particulate field and how it interacts with the helicopter and rotor is illustrated in Fig. 3 for a case with tracer particles. The effect of the rotor flow is to accelerate the particles through the rotor plane abruptly changing their flow direction. Particles impinge on the helicopter surface and are enveloped in the surrounding boundary layers. Consistent with Fig. 2, turbulent dispersion of the particles occurs where they interact with the turbulent parts of the rotor vorticity field and the turbulent wake of the helicopter.

An interesting aspect of the particle motions is illustrated in Figs. 4 showing the paths deriving from sets of particles whose initial positions are on lines within one of the upstream circular disks. The views are, respectively, from the side and front. The effect of the motion through the rotor plane in reorienting the particles is evident in Fig. 4(a). To the extent the particle trajectories show the affects of turbulence it is confined to the region mostly below the helicopter. Thus, particles approach the top part on direct lines while those that interact with the lower surfaces often times appear to be contained within the turbulent flow surrounding the body.

The variability of the motion for particles entering the flow at the same point is illustrated in Fig. 5. Here, in views from the side and back, the extent to which the presence of turbulence disperses the incoming particles is made visible. The interaction with turbulence means that despite the repeatability of the incoming motions, the subsequent motion remains unpredictable and has the potential to bring particles to a range of possible positions along the surface of the air frame.

Some indication of the effect of Stokes number in how the particles behave in the vicinity of the helicopter is illustrated in Fig. 6. A front view of the particle motions for tracers

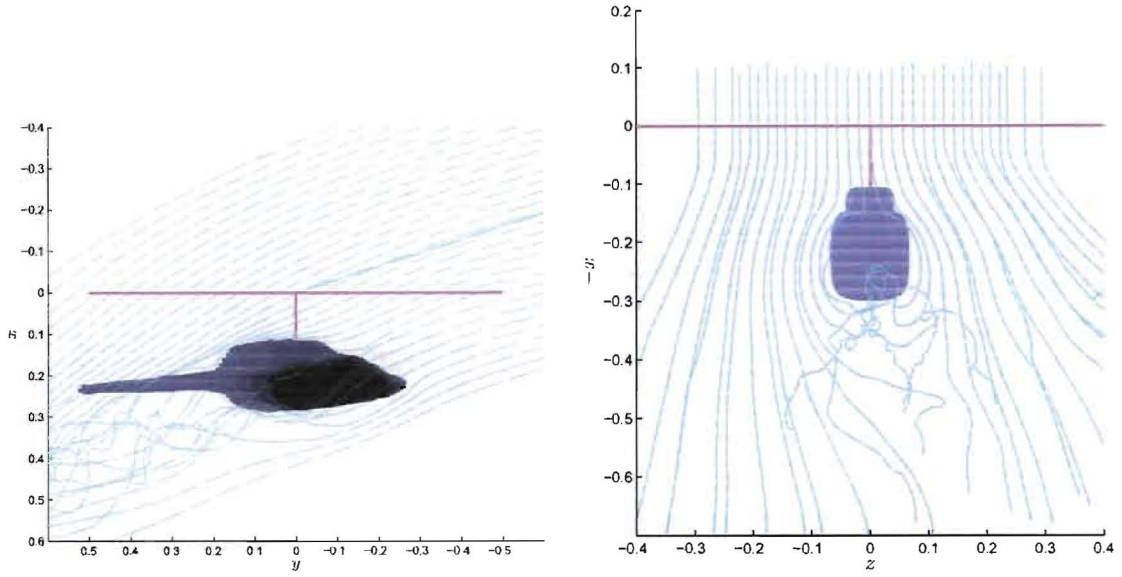

(a) Tracers originating on a vertical line.

(b) Tracers originating on a horizontal line.

Figure 4: Effect of the flow on tracers.

and for heavy particles with $S_t = 100$ are compared for the same flow field. It is seen that there are only relatively minor differences between paths during the approach to the front of the helicopter. Subsequently, as the particles negotiate around the body the heavier particles have a clear tendency to travel further below the surface before being affected by the turbulence. The effect of the latter is greater on the tracer particles. In fact, a side view would show that their trajectories are more likely to trail along parallel to the lower surface.

To find out the effect of sensor placement on the efficiency with which the upstream atmosphere can be sampled for particles it is necessary to gain information about the initial locations of particles that arrive at given points on the helicopter. For each of the nodal points that make up the helicopter surface, the collection of particles arriving within a small distance (0.01 in the present case) were computed. For each of these paths, the initial point where the particle came from within the circular disks of particle points was determined. From this the maximum distance between the initial points was computed. Figure 7 shows the percentage of locations on the airframe surface for which arriving particles have started out at varying distances. For approximately 65% of the surface points particles arrive from just a single upstream location. For a much smaller percentage of the surface points the particles arrive from positive distances apart. A very small percentage of locations are distinguished by the fact that the particles arriving there have begun from relatively far distances apart, in fact, on the order of more than half a rotor diameter.

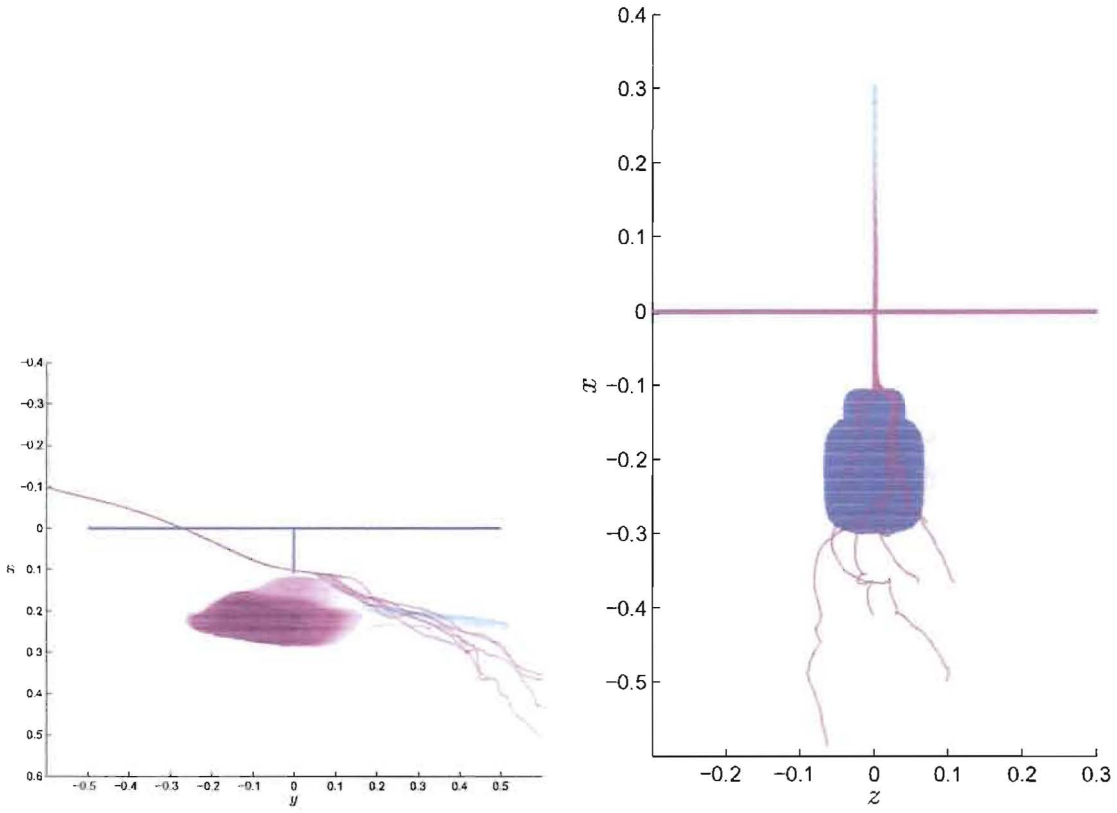

(a) Side view.

(b) Back view.

Figure 5: Particle paths with common origin.

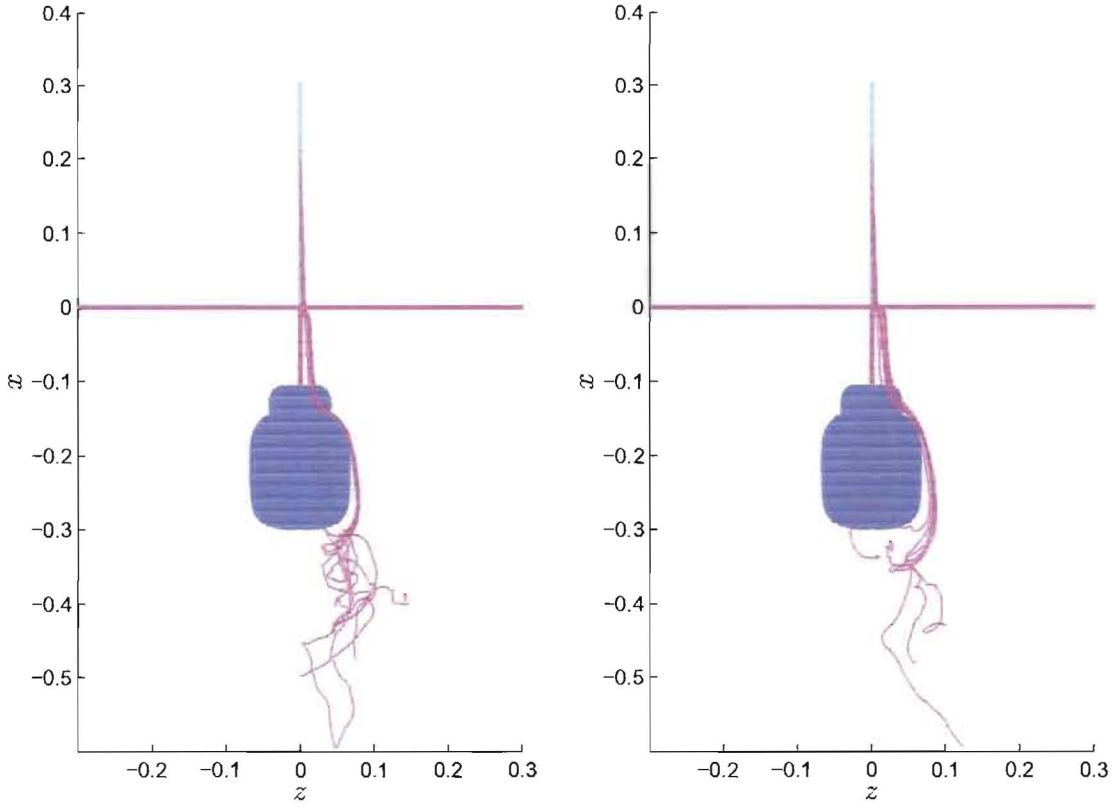

(a) $S_t = 0$.

(b) $S_t = 100$.

Figure 6: Effect of Stokes number on particle trajectories.

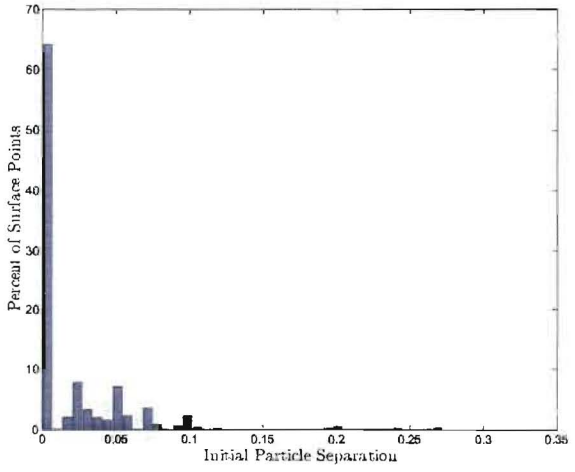

Figure 7: Percentages of the airframe surface area for which arriving particles have different magnitudes of initial separation.

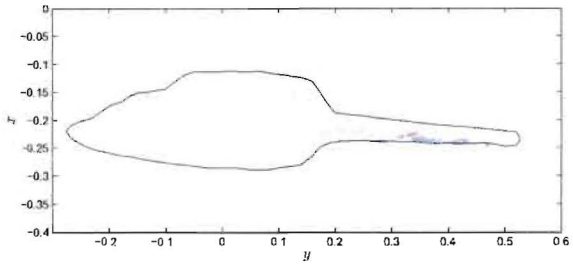

Figure 8: Surface locations for which particles arrive from disparate initial points: red, distances > 0.25; blue, distances between 0.175 and 0.25; green, distances between 0.1 and 0.175.

The plot in Fig. 8 indicates the physical locations on the helicopter where particles arrive from the largest initial separations. Particles beginning more than 0.25 apart, denoted in red, are clustered at a few points, surrounding them in blue are particles that have started out between 0.175 and 0.25 apart. There is little doubt from the results shown here that the tail section of the helicopter provides a more optimal location to efficiently sample upstream particles than the main part of the helicopter.

An explanation for the result in Fig. 8 is given in Fig. 9 showing the collection of particle trajectories that arrive at the surface points indicated in red in the former figure, (i.e. the initial particle locations are as much as 0.25 apart). The particle paths in question are seen to arrive at the tail section from two different mechanisms. In the first, they travel directly through the rotor plane to the tail region. In the second, they first approach the main section of the helicopter and then get swept up in the turbulent wake flow that carries them toward the tail section. This basic mechanism was observed in a number of different simulations, for example, computations using the actuator disk model and for massed particles with a range of Stokes numbers. Further consideration of how to optimize the placement of a particle sensor is appropriate once a specific helicopter design is to be considered. In that case, using a high resolution triangularization of the surface, showing important local features, the present code may be executed to gain comprehensive information about the particle paths. In such work it would be appropriate to investigate the expected performance of a collector in a range of flow conditions.

4 Conclusions.

A positive answer has been reached to the primary question posed in this study to the effect that the positioning of a particle collector on unmanned helicopters can potentially have a significant effect on the efficiency with which the atmosphere can be scanned for hazardous particles. For a number of test cases considered here the same basic

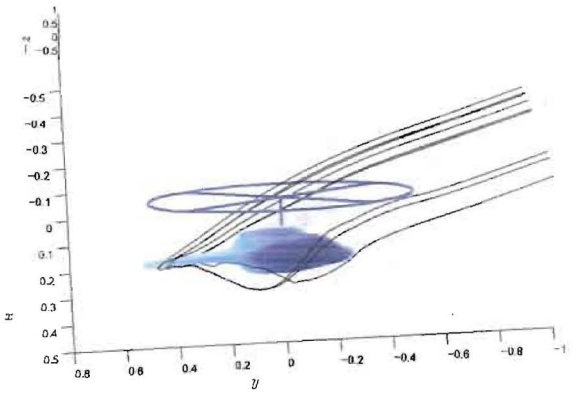

Figure 9: Paths arriving at common locations on the helicopter surface for which the initial separation is > 0.25.

physical phenomena was observed: particles that arrive at the tail section of the helicopter airframe have a greater likelihood of having come from disparate upstream positions. In effect, turbulence shed off of the helicopter in forward flight brings particles to locations in the back at the tail where they join particles that have directly approached the tail region through the rotor field. For the case of tracers and a rotor with 10 blades the upstream separation of the particles was greater than half the rotor radius. Statistics of the same order were found in other cases treated. Detailed predictions produced by high resolution simulations will be appropriate when particular air frame shapes, rotor configurations and flight conditions are investigated.

The simulations accomplished in this study are made possible by the unique qualities of the numerical scheme that was applied and developed in this project. The minimal gridding requirements in which just a surface triangularization is necessary allowed for rapid progress in implementing the methodology. The Lagrangian nature of the filament calculation dovetails well with the Lagrangian particle computations. Moreover, the capability for capturing the dynamics of shed vortical structure provides a good basis for simulating the particle dispersion that is necessary for reaching conclusions in the project. In contrast to the popularly formulated free vortex models of the rotor field that generally rely on the use of a single vortex streaming from the rotor tips [17], the present simulation utilizes an arbitrary number of filaments for each rotor - five, in the present computations. The use of multiple vortices allows for the representation of vortical structure that is essential to the physical phenomena being modeled. Moreover, solving for the rotor tip vortices as part of the general vortex filament algorithm allows for consideration of practical scenarios in which the influence of the helicopter body among many other factors is present. The conclusion may be drawn that the technology developed in this project has the potential for much wider application than the specific problem considered here. In particular, it is not hard to envisage that the VorCat scheme

can offer new capabilities in the design and analysis of helicopter flows.

5 Recommendations.

Our objectives for a Phase II continuation of this project are:

- Use VorCat simulations to optimize and evaluate the performance of particle collection technologies developed at Boeing for unmanned platforms including the Hummingbird rotorcraft and ScanEagle fixed-wing.
- Continue the development, validation and application of the VorCat platform to a range of related problems of interest to government and industry for which chem/bio hazards may be present.

The positive results of this work have raised the interest of our partners at Boeing in applying the present algorithm to studying flows associated with Boeing-specific UAV designs. In these cases, the use of high resolution surface grids can be employed that will allow for many of the details of the flow field to be accounted for numerically. If also a particular type of airborne particle is considered then simulations around realistic air frames using realistic particles can be accomplished. Additionally, a range of possible flight conditions can be considered. This kind of engineering study can be coupled with physical experiments (wind tunnel and/or flight tests) carried out by Boeing during Phase II and/or Phase III work yielding a means for optimizing the particle collection technologies employed on Boeing aircraft.

The continuation of our Phase I study into Phase II will allow VorCat, Inc. to (i) complete the development and testing of a unique, valuable flow simulation tool that will have a high probability of being purchased by a major DOD contractor such as Boeing, (ii) prove the superiority of the VorCat software over other currently available technologies for use in similar applications and, consequently, (iii) provide VorCat with the opportunity to extend its reach into other DOD and industrial applications that are closely related to the applications discussed in this report.

References

[1] Anderson, G. P. et al. "Biological agent detection with the use of an airborne biosensor," *Field Analyt. Chem. Technol.* **3**, 307-314, 1999.

[2] Bernard, P.S. and Wallace, J.M. *Turbulent Flow: Analysis, Measurement and Prediction*, John Wiley & Sons, 2002.

[3] Bernard, P. S., Collins, J. P. and Potts, M., "Vortex method simulation of ground vehicle aerodynamics," *SAE Transactions Journal of Passenger Cars - Mechanical Systems*, 612 - 624, 2005.

[4] Bernard, P.S. "Turbulent flow properties of large scale vortex systems,"' *Proc. Nat. Acad. Sci.*, **103**, 10174-10179, 2006.

[5] Bernard, P. S. "Gridfree simulation of the spatially growing turbulent mixing layer," *AIAA J.*, **46**, 1725-1737, 2008.

[6] Bernard, P. S. "Vortex filament simulation of the turbulent coflowing jet," *Phys. Fluids*, **21**:025107, 2009.

[7] Bernard, P. S., Collins, P. and Potts, M. "Vortex filament simulation of the turbulent boundary layer," AIAA-2009-3547, presented at the 19th AIAA Computational Fluid Dynamics Congress, San Antonio, Texas, June, 2009.

[8] Bernard, P. S., Collins, P. and Potts, M. "Vortex filament simulation of the turbulent boundary layer," *AIAA J.*, to appear, 2010.

[9] Chorin, A. J., "Hairpin removal in vortex interactions II," *J. Comput. Phys.* **107**, 1 - 9, 1993

[10] Chorin, A. J., *Vorticity and Turbulence*, Springer-Verlag, 1994.

[11] Fessler, J. R., Kulick, J. D. and Eaton, J. K. "Preferential concentration of heavy particles in a turbulent channel flow," *Phys. Fluids* **6**, 3742 - 3749, 1994.

[12] Gooding, J.J. "Biosensor technology for detecting biological warfare agents: Recent progress and future trends," *Analytica Chimica Acta* **559**, 137-151, 2006.

[13] Greengard, L. and Rokhlin, V., "A fast algorithm for particle simulations," *J. Comp. Phys.* **73**, 325 - 348, 1987.

[14] Gursul, I., "Vortex flows on UAVs: Issues and challenges," *Aeronautical J.* **108**, 597 - 610, 2004

[15] Hill, A., "Modeling concentration profiles of chemical warfare agents to assess the usefulness of airborne chemical detectors," Defense Science and Technology Organisation, Technical Note DSTO-TN-0506, 2003.

[16] Hogan, R. C. and Cuzzi, J. N. "Stokes and Reynolds number dependence of preferential particle concentration in simulated three-dimensional turbulence," *Phys. Fluids* **13**, 2938 - 2945, 2001.

[17] Leishman, J. G., Bhagwat, M. J. and Bagai, A., "Free-vortex filament methods for the analysis of helicopter rotor wakes," *J. Aircraft*, **39**, 759-775, 2002.

[18] Lynn, R. and Gursul, I., "Vortex dynamics on a generic UCAV configuration." AIAA-2006-61 44th AIAA Aerospace Sciences Meeting and Exhibit. Reno, Nevada. Jan. 9-12, 2006.

[19] Naimushina, A. N. et al. "Airborne analyte detection with an aircraft-adapted surface plasmon resonance sensor system," *Sensors and Actuators B: Chemical* **104** 237-248,

[20] Nair, M. L. "Conceptual design, engineering modeling, and experimental validation of air sampling system for chemical sensor insertion into the U.S. Army Research

Laboratory's (ARL) silent operating aerial reconnaissance (SOAR) program," ARL Report A963124, 2004.

[21] Puckett, E. G., "Vortex methods: an introduction and survey of selected research topics." In M.D. Gunzburger and R.A. Nicolaides, editors, *Incompressible computational fluid dynamics: trends and advances*, Cambridge University Press, 335 - 407, 1993.

[22] Squires, K.D. and Eaton, J. K., "Preferential concentration of particles by turbulence," *Phys. Fluids A* **3**, 1169, 1991